Space Weather Effects on Communications Satellites

H.C. Koons
J.F. Fennell

Abstract

Space near Earth contains a hostile environment for spacecraft. Satellites in space are exposed to such hazards as single-event effects from cosmic rays, internal charging from Van Allen radiation belt electrons, and surface charging from energetic electrons in hot plasma injected into the inner magnetosphere during geomagnetic storms and substorms. These geophysical phenomena are highly variable, and are collectively known as space weather. Problems associated with these hazards include loss of mission, subsystem failure, mission degradation, loss of data, phantom commands, spurious signals, and single-event effects (upsets, latchup, and burnout). Here, we describe the physical phenomena and give numerous examples of their effects on communications satellites.

1. Introduction

When Arthur C. Clark first described the principles for satellite communications from "stations" in geostationary orbit in 1945 [1], there was no such concept as space weather. Today, the space environment (frequently called space weather, in analogy to terrestrial weather) is a major cause of anomalies on communications satellites in geosynchronous orbit [2-8]. Just as terrestrial weather is determined by the seas, mountain ranges, continents, and the polar and equatorial regions, the space weather environment is determined by the plasmas, particles, and magnetic fields in the different regions of space. Each of these can be highly variable, and one must have a basic understanding of these phenomena and of their interaction with satellites in order to understand their differing effects on space systems [2, 9]. Space weather is especially important because human enterprise is increasingly dependent on communication satellites for business data, military operations, news, advertising, entertainment, and business or personal contacts via phone, fax, and video conferences via the Internet.

Satellites in space are exposed to numerous environmental hazards, such as single-event upsets from solar and galactic cosmic rays, internal charging and excessive radiation doses from the Van Allen radiation belt particles, surface charging by hot plasmas energized during geomagnetic storms, collisions with meteoroids and debris, surface damage from atomic ions impinging on the surface, and drag from the neutral atmosphere. The most serious hazards include single-event effects, surface charging, and internal charging. The most serious problem caused by these hazards is the entire loss of a satellite's function, sometimes called loss of mission. Other impacts include subsystem failure, mission degradation, loss of data, phantom commands, spurious signals, safeholds, and latchups, and indirect impacts, such as increased cost of operations, loss of revenue, cost of redesign, etc. [2].

Some space weather effects that are not necessarily considered anomalies include normal solar cell and surface degradation, and expected gravitational, magnetic, thermal, plasma, particulate, and optical effects. Problems in these areas beyond those planned into the satellite's design, however, are considered to be anomalies.

Most of the above will be covered in this paper. The effects on communications satellites will be used as examples of the most important hazards.

2. The Space Environment

We will begin with a relatively simple overview of the space environment, emphasizing the variable weather phenomena that interact with spacecraft. It is a rather daunting list, if you have thought of space as mainly an empty vacuum. We will leave most of the details until we discuss the specific hazards below.

J. F. Fennell is with the Space Science Applications Laboratory, The Aerospace Corporation, 2350 E. El Segundo Blvd., El Segundo, CA, USA 90245; Tel: +1 (310) 336-6519; Fax: +1 (310) 336-1636; E-mail: Joseph.F.Fennell@aero.org.

H. C. Koons passed away after completing this paper.

This is one of the invited Commission H *Reviews of Radio Science*.

2.1 The Sun

The sun is ultimately responsible for many hazards to spacecraft. Particulate radiation in the form of solar cosmic rays (very energetic protons and heavier atomic nuclei of solar origin), eruptive prominences, and coronal mass ejections are sporadic energetic events that can produce hazardous environments and satellite anomalies when the radiation reaches the Earth's vicinity. The sun is also a source for X-rays from some solar flares and for radio noise. These are not significant hazards to spacecraft.

The Earth is in the region of space controlled by the outflow of plasma from the sun. This region is called the heliosphere. The plasma outflow, which consists primarily of thermal protons and electrons, is called the solar wind. It has a highly variable speed and density. It also contains a magnetic field that originates in the upper region of the sun's corona, and is frozen into the solar-wind plasma as it flows outward. The solar-wind plasma is not energetic enough to be a direct hazard. The solar wind is the source of radio emissions that are also not considered to be a hazard.

Solar particle events cause single-event effects and solar-array degradation on spacecraft. Spacecraft surface charging occurs during magnetic storms. Magnetic storms are disturbances in the geomagnetic field driven by the interaction of the solar wind with the Earth's magnetic field. They occur when coronal mass ejections, shockwaves, and high-speed solar streams strike the magnetosphere. Spacecraft internal charging occurs when the radiation-belt fluxes increase following magnetic storms. Atmospheric drag increases when solar X-rays and currents in the ionosphere, driven by geomagnetic storms, heat and raise the height of the neutral atmosphere.

2.2 Galactic Sources

The heliosphere moves through the interstellar medium with the sun. The interstellar medium is the region between the stars. It contains very-low-density plasma, galactic cosmic rays, and electromagnetic radiation from distant stars and galaxies. Galactic cosmic rays are very-high-energy atomic nuclei. The most energetic are believed to be produced in supernova and radio galaxies. The galactic cosmic rays have sufficient energy to penetrate into electronic boxes and to cause upsets to virtually all microprocessors, memory chips, gate arrays, etc. It is amazing to realize that they have traveled for perhaps millions of years before slamming into the electronics on a spacecraft.

2.3 Earth's Magnetosphere

The Earth is protected from the direct impact of the solar wind and from lower-energy solar particles by a teardrop-shaped cavity around the Earth called the magnetosphere. Figure 1 shows an artist's concept of the magnetosphere. It is formed by the interaction of the solar wind with the Earth's magnetic field.

The outer boundary of the magnetosphere is known as the magnetopause. The magnetopause is an electrical current layer that, to a first approximation, entirely confines the Earth's magnetic field. The magnetopause forms where the dynamic pressure of the solar-wind plasma balances the static pressure of the geomagnetic field. Since the solar-wind speed is supersonic, a detached shock appears in front of the magnetosphere. This shock is called the bow shock. The region between the bow shock and the magnetopause is known as the magnetosheath. It is about two Earth radii

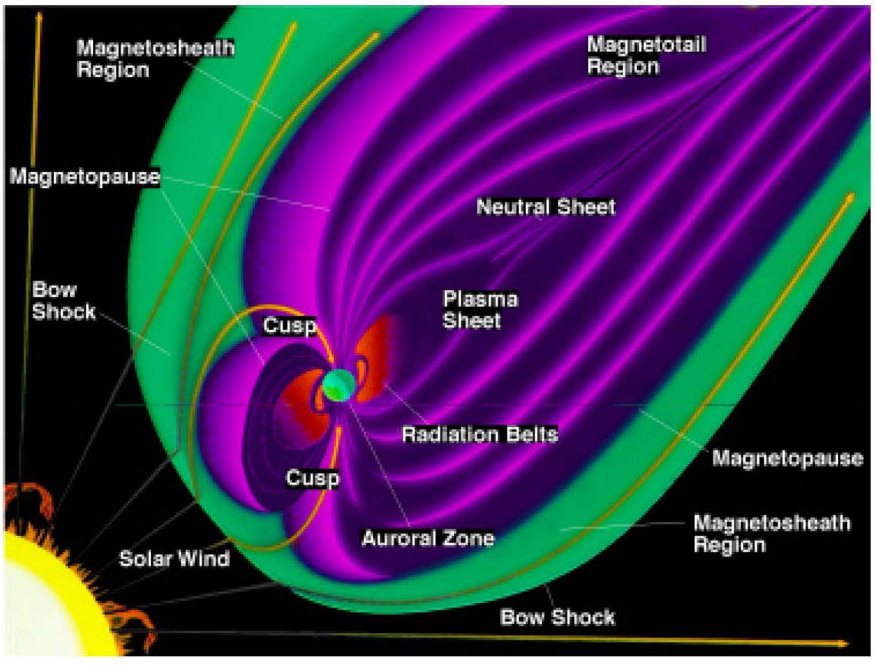

Figure 1. The internal structure of the Earth's magnetosphere (courtesy of Goddard Space Flight Center).

wide along the Earth-sun line, and is a region of considerable plasma turbulence. Along the Earth-sun line, a typical geocentric distance to the magnetopause from the center of the Earth is 10 Earth radii. Occasionally, when the solar-wind velocity is quite high, the distance can be less than 6.6 Earth radii (the distance from the center of the Earth to geosynchronous orbit), and satellites in geosynchronous orbit on the sunward side of the Earth may find themselves in the magnetosheath, outside of the magnetopause. The energy of the particles in the magnetosheath is too low to be a hazard to spacecraft.

Charged particles inside of the magnetosphere are influenced by the Earth's internal magnetic field. This magnetic field is driven by dynamo processes in the Earth's molten core. To a first approximation, the field in the inner magnetosphere is that of a dipole. The magnetosphere contains the Van Allen radiation belts, the plasma sheet, the plasmasphere, the magnetotail, and a number of other uniquely identifiable regions. Several of the regions inside of the magnetosphere provide unique hazards to spacecraft.

Some solar-wind plasma is energized and transported inside of the magnetosphere under the influence of the electric field imposed on the magnetosphere by the interaction of the solar wind with the geomagnetic field. Once inside, it forms different populations with different characteristics. Plasma regions are separated from their neighbors by a boundary on which current flows. Current also flows along and across geomagnetic field lines. These currents give rise to a magnetic field that significantly modifies (distorts) the shape of the dipolar field in the outer magnetosphere. These currents also vary with time, giving rise to significant magnetic-field fluctuations. Stronger disturbances are called magnetic storms.

Since the electrons and protons in the magnetosphere gyrate around and move rapidly along the geomagnetic field lines, the space particle environment is organized by the magnetic field. Magnetic field lines near geosynchronous altitudes map down to the northern and southern polar regions. Electrons from the hot plasma precipitate into the atmosphere in the auroral regions at both ends of the field lines, i.e., the northern and southern auroral zones, generating the optical displays seen there. Processes at low altitudes also accelerate the auroral electrons.

3. Environmental Hazards

3.1 Single-Event Effects

3.1.1 Description

A single energetic ion, such as a cosmic-ray iron nucleus or a trapped energetic proton, can interact with a microelectronic circuit in a manner that causes a change in the operation of the circuit [10, 11]. The energetic ion loses energy as it ionizes atoms in the device along the track it traverses. This creates free charge pairs, which are known as electron-hole pairs, along the ion track. The electric fields in the device sweep up these charges and generate a signal in the device, changing its state. An ion can also undergo a nuclear interaction with the atoms in the device. This generates a shower of energetic nuclei that then suffer ionization losses. Barillot and Calvel [12] have reviewed single-event effect (SEE) occurrences in commercial spacecraft.

The composite cosmic-ray spectrum represents a combination of galactic cosmic rays and solar cosmic rays [13, 14]. The cosmic-ray flux is highly variable at energies below 10 GeV/nucleon. The variability has two sources: (1) the changes of the galactic cosmic-ray access to the near-Earth space during the solar cycle (see Section 4.3), and (2) the enhancement of the cosmic-ray flux caused by energetic solar-particle events. The latter produces the most intense overall flux.

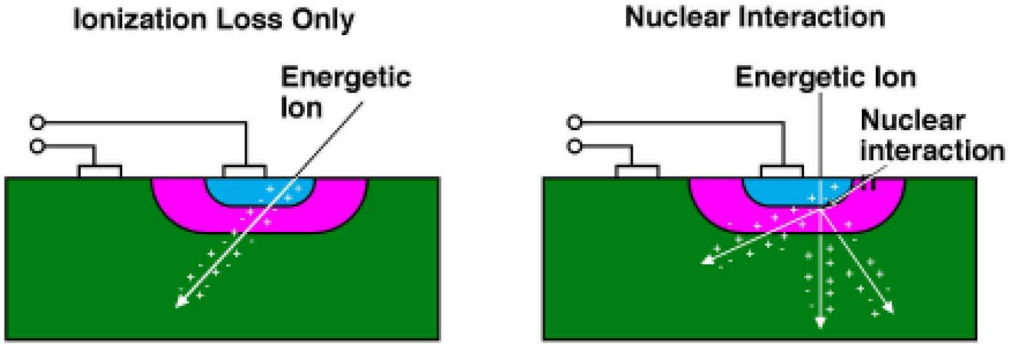

Figure 2. Examples of single-event effects: electrons and holes are swept up by the electric field in the depletion region (the lightest shading, in pink in the color version), resulting in a single-event effect.

3.1.2 Types of Single-Event Effects

All of the different effects caused by the interaction of an energetic ion with a device are collectively known as single-event effects (SEE). Historically, the different types of single-event effects have been identified by the response of the microelectronic device. Examples are shown in Figure 2.

When the free charges created by an ion are collected at the circuit's source and drain points, a current pulse occurs. The pulse can be as large as that produced by a normal input signal. The spurious pulse may change the state of the device. When this happens, the change of state is called a single-event upset (SEU). This can result in the change of a value held in a memory device, such as an instruction in a microprocessor chip, data in a memory chip, an address in an address register, etc. A single-event upset implies that there is no permanent damage done to the circuit. The single-event upset may be self-correcting, depending on the device and how it is operated.

In a single-event latchup (SEL), the free charges created by the ion interact with the parasitic transistors that often exist in microelectronic devices. A latchup can occur when the spurious current spike produced by the free charges activates the parasitic transistors, which combine into the circuit with large positive feedback. The circuit turns fully on, causing a short across the device. The short continues until the device fails (burnout), or until the power is cycled. A single-even latchup can cause permanent damage to a device, including total failure.

The free charge created by the ion in an analog device can cause a voltage spike at the output of the device. Depending on the speed of the amplifier and the following circuitry, the spike can be propagated to other circuits and cause errors. Such errors are called single-event transient effects.

Depending on the structure and function of the microelectronic device, the effect caused by the free charges can show up as normal but unwanted responses from the device. This is especially true for very complex devices such as microprocessors. For example, a single-event upset may cause the execution of an allowed, but inappropriate, instruction by a microprocessor, such as the halt instruction. Devices that have an on-chip diagnostic mode that was only intended for factory use have entered the diagnostic mode as a result of a single-event effect. This means that the device is not performing its intended purpose in the system until the error is corrected. In extreme cases, the device may enter a mode which is destructive, such as can occur with a single-event latchup.

3.1.3 Characterization of Single-Event-Effect Sensitivity

The sensitivity of an electronic device to the free charges that are generated by energetic ions passing through it determines its single-event-effect response. The sensitivity is measured in terms of the effective cross section for upsets per particle per unit area of the device. This cross section depends on the energy loss rate of the ions traversing it. The amount of energy lost by the ion per unit path length in the device is called the linear energy transfer (LET).

The linear energy transfer depends on the type of ion and its energy. Most devices require a minimum linear energy transfer to cause an upset. This minimum is called the threshold linear energy transfer. For most devices, the cross section for an upset increases with increasing linear energy transfer, up to a knee value. Devices with a low linear-energy-transfer threshold (i.e., <10 ions/m^2-sr-sec-MeV/nucleon) can be upset by low-mass high-energy ions, such as protons, helium, oxygen, etc.

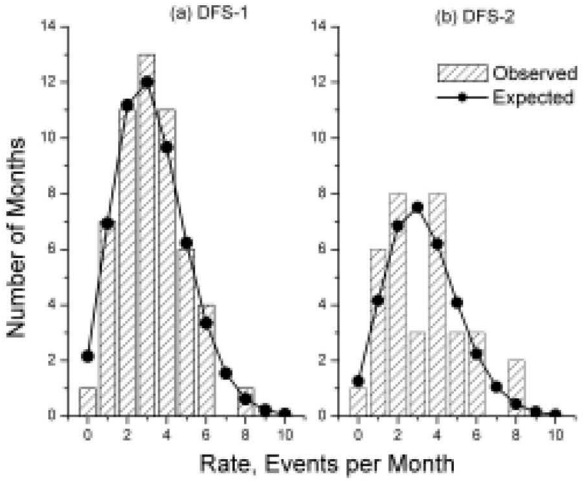

Figure 3. The distribution of single-event upsets on (a) MILSTAR DFS-1 and (b) MILSTAR DFS-2. The expected curve is based on a Poisson distribution (adapted from [15]).

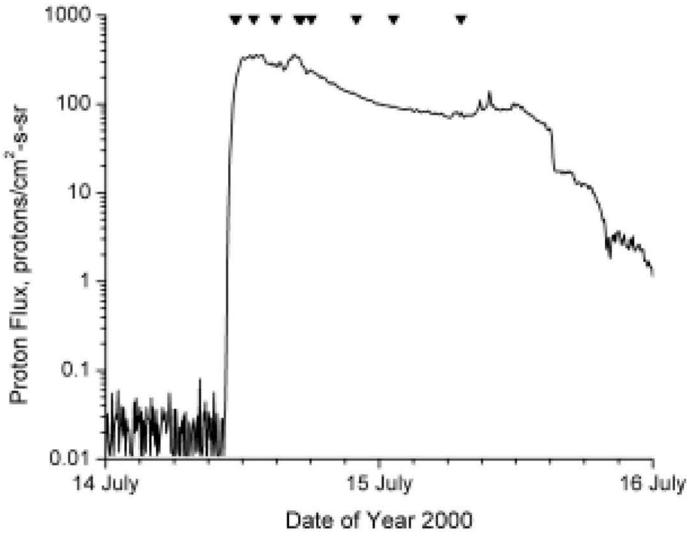

Figure 4. Inverted triangles mark the times of single-event upsets on spacecraft in high-altitude obits during the solar proton event of July, 2000. The time profile of the > 50 MeV protons, measured by the GOES-8 spacecraft during the event, is also shown (proton data courtesy of NOAA).

3.1.4 Anomalies Caused by Single-Event Effects

3.1.4.1 Galactic Cosmic Rays

The MILSTAR DFS-1 and DFS-2 military communication satellites were launched into geosynchronous orbit in February, 1994, and November, 1995, respectively. A database was created to analyze the in-situ occurrence of single-event upsets on the two essentially identical spacecraft. It was found that the upset rate varied from zero to eight upsets per month on each vehicle, with an average of 3.2 upsets on DFS-1 for the first 174 months in orbit, and an average of 3.3 upsets on DFS-2 for the first 112 months in orbit [15].

Single-event upsets caused by galactic cosmic rays should be distributed in time according to a Poisson distribution, because their occurrence can be described as a random variable with a rate that is the number of occurrences per unit time. The Poisson distribution has a single parameter, which, in this case, is interpreted as the average number of occurrences per month. In [15], a chi-squared goodness of fit test was used to see if the distribution of upsets satisfied a Poisson distribution. The hypothesis that the distribution is Poisson is accepted if the value of chi-squared is less than the value at the 0.05 significance level. Figure 3 shows the histograms of the number of months each upset rate occurred as a function of the rate for both spacecraft. Although the average numbers of upsets per month were virtually identical, the significance level from the chi-squared test gave a high value of 0.98 for DFS-1, but a low value of 0.23 for DFS-2. Figure 3 shows that the largest deviations from the expected distribution for DFS-2 occurred at three and eight upsets per month. However, the low value of the significance level for DFS-2 did not imply that the occurrences on DFS-2 did not fit a Poisson distribution. Since the significance level for DFS-2 was still much greater than our acceptance level of 0.05, the hypothesis that the distribution was Poisson can not be rejected. If 100 identical vehicles were launched, statistically, one would expect that about 20 would have worse fits than DFS-2, with a similar number of single-event upset occurrences.

3.1.4.2 Solar Cosmic Rays

Solar particle effects are caused by energetic events, such as solar flares and shocks. They can produce a significant flux of energetic protons and heavier particles. An energetic event can include ions with energies above 100 MeV. Since protons dominate such particle events [14], they are frequently called solar proton events. The larger energetic events cause single-event effects on spacecraft, and they also make a significant contribution to solar-array degradation.

The temporal profile of a solar proton event is determined by the relative positions of the particle emission region and the solar magnetic flux tube that is connected to Earth: the more directly connected, the faster the risetime and the shorter the event. A solar proton event has a proton flux of at least 10 proton flux units (pfu), where 1 pfu = 1 proton/cm^2-s-sr at energies greater than 10 MeV. Energetic solar particles can cause single-event effects on spacecraft, especially during strong ($\geq 10^3$ pfu), severe ($\geq 10^4$ pfu), or extreme ($\geq 10^5$ pfu) solar particle events [16]. The upside-down triangles on Figure 4 show the times of such upsets on spacecraft in geosynchronous and Molniya orbits, during the solar proton event of July, 2000.

3.1.4.3 Inner Radiation Zone and South Atlantic Anomaly

Solar and galactic cosmic rays are the primary source of singe-event effects for electronics that are moderately radiation hardened. Soft parts – that is, parts with low linear-energy-transfer thresholds – can also experience single-event effects from energetic protons. The cosmic-ray flux with linear energy transfer = 10 ions/(m^2-sr-sec-MeV/nucleon) is relatively low. However, the trapped high-energy proton fluxes in the inner radiation belts with this linear energy transfer can be very intense, exceeding 10^8 protons/(m^2-s-sr) for energies > 50 MeV [17]. Programs that plan to fly satellites with low- to middle-altitude orbits or low perigees have to take this into account when developing their systems.

Normally, the inner radiation zone is avoided because the total radiation dose is so large there. However, some low-altitude missions still experience effects from the energetic protons in a region known as the South Atlantic Anomaly. The asymmetries in the geomagnetic field cause the radiation belts to "dip" closer to the Earth in the south Atlantic regions, and satellites that pass through this region can experience single-event effects.

From September, 1988, to May, 1992, UoSAT-2, an amateur-radio communications satellite, flying in a polar orbit at ~ 690 km altitude, experienced almost 9000 single-even upsets (SEUs). The majority of these (75%) occurred in the South Atlantic Anomaly (SAA) region. Figure 5 shows the spatial distribution of upsets on UoSAT-2. The region of the South Atlantic Anomaly is clearly indicated by the high occurrence of upsets over the South American continent and South Atlantic ocean. Events at higher latitudes were attributed to galactic cosmic rays and solar protons [18].

3.2 Surface Charging

3.2.1 Description

Surface charging is the accumulation of electrons from the space environment on the surface of a spacecraft. As electrons accumulate on the surface, they repel lower-energy electrons approaching from the plasma. This ultimately limits the potential to which the surface can charge with respect to the plasma. Since a satellite is essentially always immersed in a space plasma – whether it be in the ionosphere, magnetosphere, or the solar wind – the surface of a spacecraft always charges with respect to the plasma to a potential called the floating potential. This floating potential is a monotonic function of the plasma's temperature. However, charging to large negative values with respect to the plasma is determined by the secondary-emission properties of the surface material, and has been shown to correlate directly with the flux of electrons with energies greater than 30 keV [19]. In the ionosphere, the thermal energy is typically a few eV, while in the plasma sheet, it can be as high as 10 to 20 keV.

If the surface material is an insulator or a conductor isolated from the spacecraft frame, the charges may reside on the surface (or just below the surface) for a long period of time. If the material is a poor conductor or a dielectric, the charges will slowly bleed off to ground (the satellite frame) or to surrounding materials. If the material is a grounded conductor, the surface charges rapidly, and equilibrates with the spacecraft frame.

The floating potential is the potential at which the net current to each surface element on the spacecraft is zero. This is the point at which it is in equilibrium with the

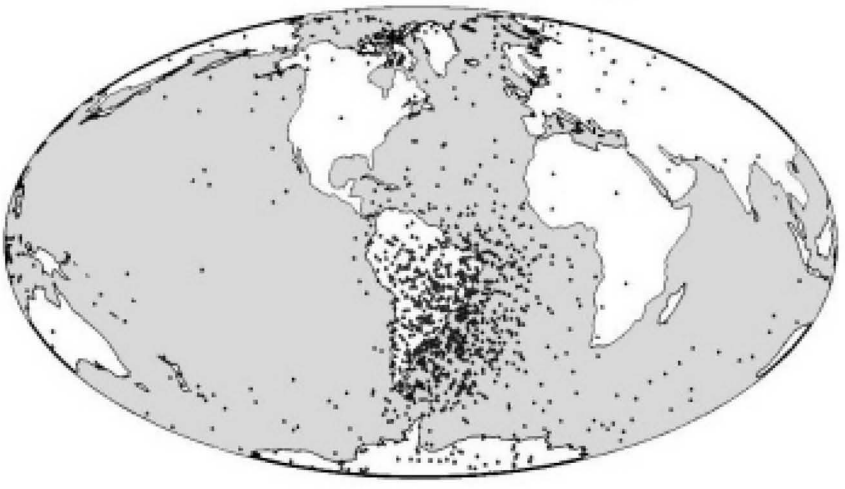

Figure 5. Single-event upsets on the low-altitude UoSAT-2 amateur-radio communications satellite. The majority, from protons in the inner radiation belt, occur in the South Atlantic Anomaly over South America and the South Atlantic Ocean. Upsets scattered over the rest of the globe are from galactic cosmic rays [6] (courtesy of NOAA).

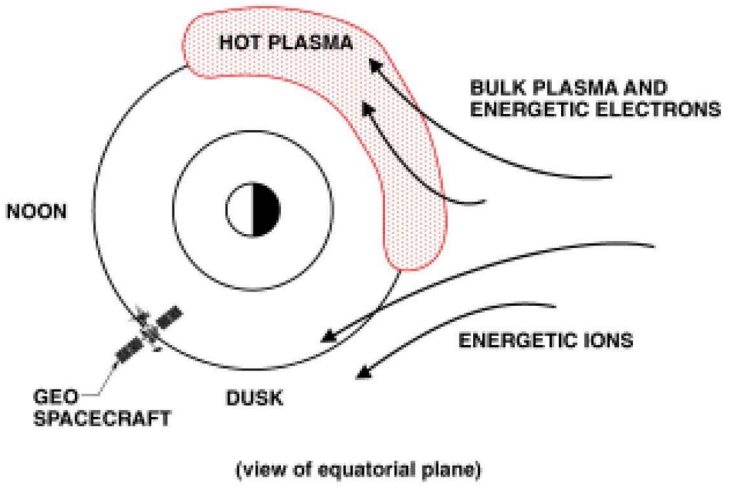

Figure 6. An artist's conception of the region in geosynchronous orbit where hot plasma can cause surface charging (after [25]).

plasma. This can be quite a complex current balance because of the number of different currents involved. For an object as simple as a conducting sphere, the currents include not only the thermal ions and electrons in the plasma, but also secondary electrons that leave the surface when a primary ion or electron strikes it, and photoelectrons that leave the surface when it is struck by photons from the sun. Because the surface is made of materials with differing electrical properties, the current balance and thus the floating potential of each surface element can be different. This generates a differential potential between the spacecraft frame and each material, and between adjacent materials with different electrical properties.

Under most circumstances, the floating potential and the differential potentials are small, and pose no hazard to the vehicle. However, during storms, hot plasmas, with temperatures between 1 and 20 keV, envelop the spacecraft. Dielectric surfaces are then charged to differential potentials as high as 10 kV. This phenomenon is known as surface charging. If the electric field arising from these differential potentials exceeds the breakdown strength for the material, either along the surface or through the material to the spacecraft frame, then an electrostatic discharge (ESD) occurs. The electromagnetic interference and currents resulting from such discharges pose a significant hazard to spacecraft electrical systems. A recent study showed that surface charging is the leading environmental cause of spacecraft mission failures [7].

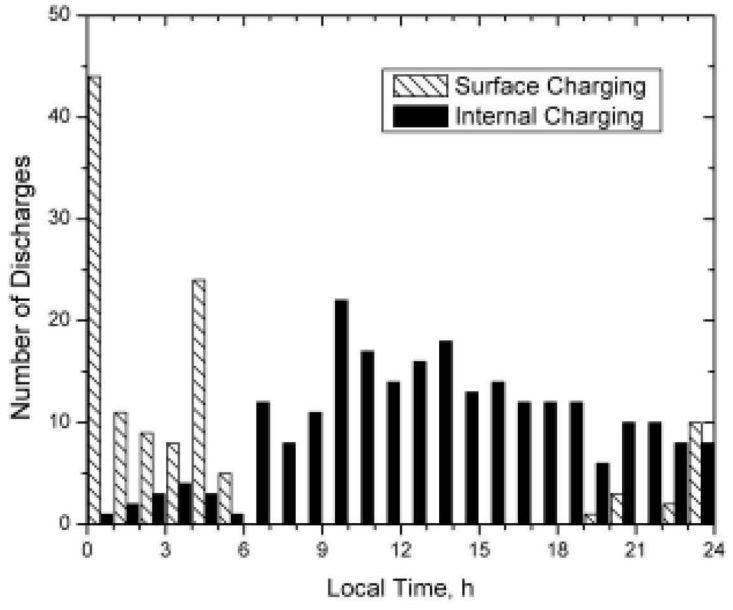

Figure 7. A histogram of the number of occurrences of electrostatic discharges due to surface charging and internal charging on the SCATHA satellite as a function of local time at the spacecraft (adapted from [21]). The data are from a total of 1527 days, between February, 1979, and March, 1988 (reprinted with permission of the American Institute of Aeronautics and Astronautics, Inc.).

3.2.2 Surface Charging in Various Orbits

3.2.2.1 Geosynchronous Orbit

Surface charging in geosynchronous orbit primarily occurs during substorms. During a substorm, the electrons are heated at distances of ~ 20 Earth radii in the magnetotail, and are driven inward toward the Earth. This injection is caused by the rapid acceleration of the electrons by an inductive electric field, generated by the motion of the geomagnetic field as it snaps back to its normal dipolar configuration from a stressed configuration. This primarily occurs on the night side of the Earth. The electrons envelop spacecraft in high-altitude orbits, such as geosynchronous orbit, and those in HEO and MEO orbits on field lines that connect to this region of space. The region where the hot plasma is normally encountered in geosynchronous orbit is shown in Figure 6. Its limits in local time have been measured to be from ~ 19 h LT through midnight to ~ 9 h LT. Surface charging primarily occurs from pre-midnight to local morning, because the energetic electrons drift from their injection point toward dawn.

The first spacecraft mission believed to be lost by a surface-charging anomaly was DSCS-II (9431) on June 2, 1973. It failed when power to its communication subsystem was suddenly interrupted. A review board found that the failure was due to a discharge caused by spacecraft charging as a result of a geomagnetic substorm [20].

Figure 7 shows the local-time distribution of electrostatic discharges due to surface charging on the SCATHA spacecraft [21]. The discharges were attributed to surface charging because, in each case, the Surface Potential Monitor aboard the spacecraft indicated that the dielectric samples on the surface of the vehicle were charged to a relatively high value when these discharges were observed.

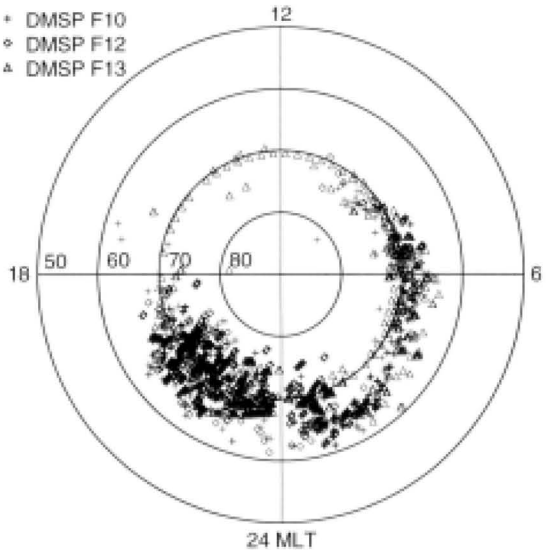

Figure 8. The location in magnetic latitude and magnetic local time of surface-charging events measured on the DMSP satellites at low altitude in the auroral zones [22] (courtesy of the Air Force Research Laboratory).

3.2.2.2 Auroral Zone

Magnetic field lines near geosynchronous altitudes connect to the northern and southern auroral zones at low altitudes. The energetic electrons that precipitate into the atmosphere along these field lines cause optical auroral displays, and also cause satellite surface charging on low-altitude, polar-orbiting spacecraft.

Figure 8 shows the region in LEO (low Earth orbit) where charging was observed on DMSP spacecraft [22]. Each point shows the location where the vehicle frame potential was measured to be more negative than -100 V. Each point occurred in an auroral arc. At low altitudes,

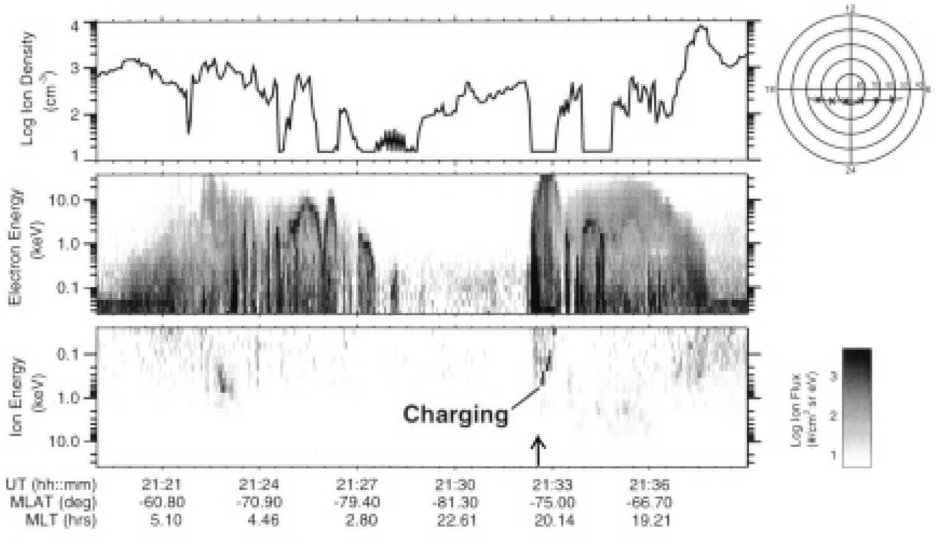

Figure 9. The environmental parameters associated with the surface-charging event and anomaly (at the arrow) on the DMSP F13 spacecraft at 21:32:40 (h:m:s) on May 5, 1995 (after [23], reprinted with permission of the American Institute of Aeronautics and Astronautics, Inc.).

charging only occurred when the vehicle was within an auroral arc. In Figure 9, an intense auroral arc occurred beginning just after 21:32 UT. The electron flux is shown in the middle panel. Within this arc, at the time shown by the arrow, an anomaly attributed to spacecraft surface charging occurred on a DMSP spacecraft [23]. At the time, the environment satisfied the three criteria required for significant charging of the spacecraft frame: (1) the integral number flux must be greater than 10^8 electrons/cm^{-2}-s-sr for electrons with energies greater than 14 keV, (2) the spacecraft must be in darkness, and (3) the background plasma density must be less than 10^{-4} cm^{-3} [24].

3.2.2.3 HEO (Molniya) Orbits

The Molniya orbit is a highly eccentric orbit (HEO), with an inclination of ~ 63° and a period of 12 h. Figure 10 shows the location of frame charging measured by a spacecraft in a Molniya orbit. Spence et al. [25] analyzed a database of approximately 100 anomalies experienced by several satellites in similar orbits. They mapped the anomalies from the location of the spacecraft at the time of the anomaly to the magnetic equator along magnetic field lines, and showed that most of the anomalies mapped to the dawn sector, between 0000 MLT and 1000 MLT. This is just the region where surface charging was seen to occur in Figure 10. Based on this mapping, they attributed these anomalies to surface charging. On a later vehicle, the same type of anomalies were shown to correlate with frame charging.

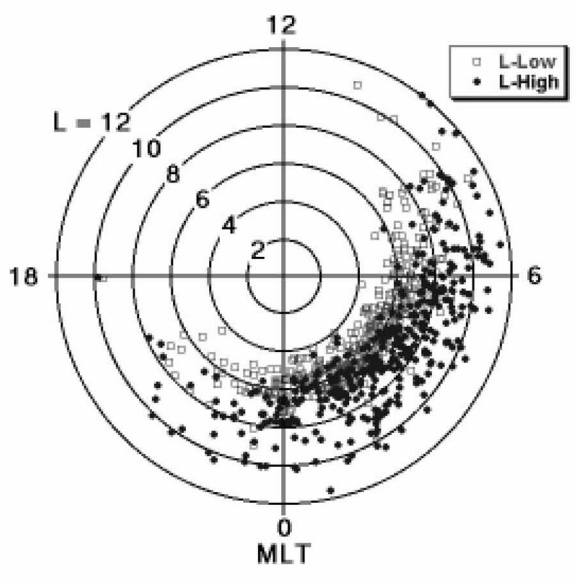

Figure 10. The location in Magnetic Local Time and L-shell where the spacecraft frame potential was less than -30 V in a Molniya orbit. The squares indicate the low L-shell limit of the charging (no data were taken below L ~ 4) and the circles show the high L-shell limit for each orbit. The points were not connected to simplify the drawing.

3.2.3 Surface Charging Mitigation and Risk

The space environment may dictate parts and materials selection in some applications and orbits. Failure to consider the environment leads to technical risks in parts and materials selection, EMC design, software and firmware design, and weight budget. Redesign, rework, and retest required by late recognition of environmental impacts may cause cost overruns and schedule delays. An example is the MARECS B spacecraft, a maritime European communications satellite. It was removed from the Ariane launch vehicle and returned to the factory for retest and rework because of a large number of environmental anomalies on MARECS A [26, 27]. Anomalies caused by the space environment increase the need for monitoring a spacecraft's state of health, increase the manpower required to operate the spacecraft, and result in inefficient workarounds when the are frequent. The most serious risk is that of subsystem or mission failure.

3.3 Internal Charging

3.3.1 Description

Internal charging is caused by energetic electrons that have penetrated into or through satellite surface material. These electrons deposit their charge on and inside cables, circuit boards, and other dielectrics, or on ungrounded conductors. Over time, the charge can build up electric fields in and between materials to breakdown levels, leading to electrostatic discharges into sensitive circuits. Internal charging is sometimes called bulk charging or deep dielectric charging. The penetrating electrons normally must have relatively high energies, i.e., > 300 keV. In geosynchronous orbit, the peak fluxes of the penetrating electrons occur two to five days after a magnetic storm, or after the onset of a high-speed solar-wind stream. Discharges have occurred on spacecraft for enhanced electron fluence levels in the range from ~ 3 ´ 10^9 to 10^{12} electrons/cm^2 in a few hours to days.

Internal charging occurs where the energetic electron fluxes are high. This occurs along field lines with L values in the range of $3 < L < 7$. The fluxes are highest where the L value is lowest in this range. The L value is the distance in Earth radii from the center of the Earth to the point at which a magnetic field line crosses the magnetic equator, measured in the magnetic equatorial plane. Energetic electrons drift around the Earth on paths of constant L value.

Internal charging causes logic errors, phantom commands, erroneous data, electronic noise, and, in some cases, loss of device, subsystem, or system functionality. Most of the time, the results of internal charging are nonfatal. However, in rare cases it can cause serious harm to a spacecraft.

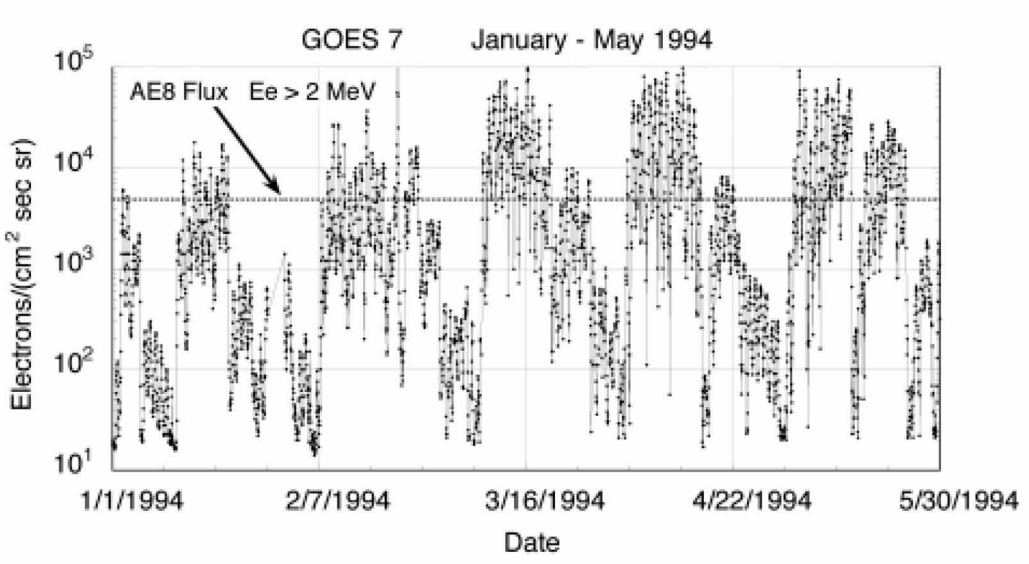

Figure 11. The daily averaged energetic electron fluxes for electrons with energies > 2 MeV from January to May, 1994 (data courtesy of NOAA). The average fluxes from the AE8 electron model are shown for comparison [28].

In geosynchronous orbit, the local time distribution of electrostatic discharge due to internal charging shows a peak in the relative occurrence coincident with a peak in the electron flux near noon [21]. The geomagnetic field is distorted at this altitude by the plasma currents that flow on the magnetospheric boundary, and a geosynchronous satellite is closest to that boundary at local noon. The causes the high-energy electron flux to be greater at noon, whereas the L value, on average, is lowest than at midnight and points in between. This flux asymmetry gives rise to the enhanced occurrence of internal electrostatic discharge around noon.

The electron fluxes in the outer radiation belt are highly variable, as shown by the example in Figure 11. The data covered a five-month period in 1994, when the solar wind consisted of a succession of high-speed and low-speed streams in a quasi-periodic manner. The electron fluxes at geosynchronous orbit generally peaked in conjunction with the high-speed solar wind streams, and dropped during the low-speed intervals. The maximum > 2 MeV electron fluxes exceeded the average flux values from the AE8 radiation-belt model [28] by more than an order of magnitude.

3.3.2 Communication Satellite Examples

A. L. Vampola [29] was the first to describe specific anomalies caused by internal charging. He identified anomalies on NTS-2 (a demonstration satellite for the Global Positioning System), Voyager 1, Meteosat-1, and DSP. The anomaly on DSP was the failure of a shutter designed to protect a sun sensor from direct exposure to the sun. The probable cause of the DSP anomaly was spurious pulses in an exposed cable, which were due to discharges in the dielectric in the cable. Based on the local time distribution of the anomalies attributed to electrostatic discharge on a number of spacecraft, Vampola estimated that half were due to surface charging and half to internal charging.

On January 20, 1994, the Anik E-2 communications satellite, owned by Telsat Canada, spun out of control because of a failure in one of its momentum wheel controllers in its guidance system. The anomaly was attributed to burnout from an electrostatic discharge to a pin on a multi-vibrator chip from an ungrounded spot shield. The primary controller and its backup both failed during this event. Service was restored using ground-based control in August, 1994 [30]. Anik E-1 suffered a similar failure in its primary controller during the same event. Full service was restored to Anik E-1 in about eight hours by successfully switching to a backup circuit.

3.4 Total Radiation Dose

3.4.1 Description

There are two basic sources of the total radiation dose for satellites flying in near-Earth space. The primary source is the radiation trapped in the Van Allen radiation belts. The secondary source is energetic protons from solar particle events. Both of these sources are highly variable. The radiation belts are populated by multiple sources. The high-energy protons in the inner radiation belt are derived from cosmic-ray albedo neutrons, created when cosmic rays strike the atmosphere, and from transient injections of solar and outer-belt protons during large storms. In addition, some energetic, anomalous, cosmic-ray ions are captured by charge exchange as they are passing near the Earth. The ionic component of the outer radiation belt has two sources: transport inward from the solar wind, and up-flow from the

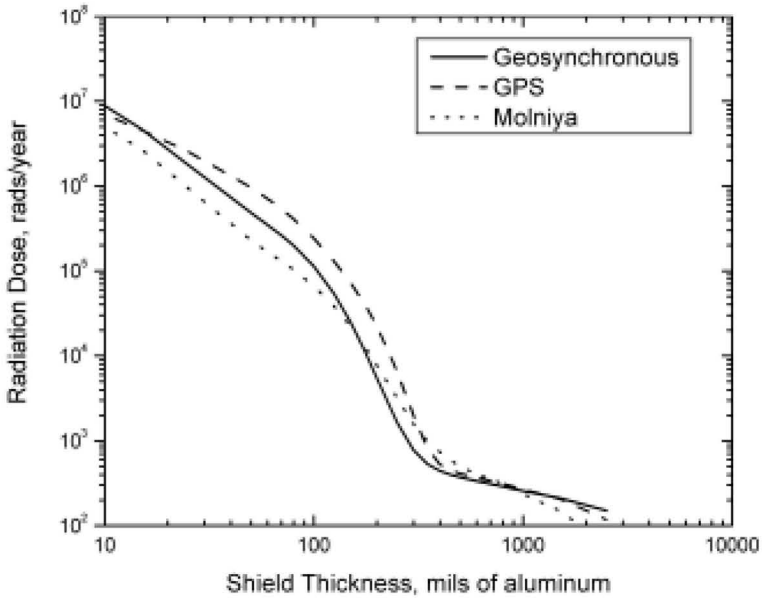

Figure 12. The yearly total radiation dose (one-half the dose at the center of an aluminum sphere) as a function of the shielding thickness for three typical orbits.

Earth's ionosphere. Most electrons in the radiation belts are of solar-wind origin, and come from the plasma-sheet plasma that is transported toward the Earth from the magnetotail by convection and fluctuating electric and magnetic fields. The complete story as to how this happens is still unfolding.

3.4.2 Radiation Protection and Radiation-Belt Models

Protection from ionizing radiation is provided by the use of electronic components (radiation-hardened parts) that are specifically designed to tolerate the environment, and by shielding. Radiation hardening requires manufacturing processes that are different from those used in commercial foundries [31]. For example, nonstandard starting materials, incorporating epitaxial layers or insulating substrates, may enhance radiation immunity. Proprietary procedures, involving novel implants or modifications of layer thickness, are also used. A new technique, known as radiation hardness by design, RHBD, uses circuit-design strategies to mitigate damage from total radiation dose and upsets and data loss from single-event effects. Radiation hardness by design includes such strategies as using multiple circuits with voting logic and redundant transistors. Parts from foundries dedicated to the production of radiation-hardened parts can cost as much as 100 times more than the equivalent commercial parts, because of their complexity and the small space-electronics market.

Models that specify the average particle environment are used to estimate the long-term average dose from the trapped radiation [28, 32]. These models are used to calculate the orbit-averaged particle spectra and total fluence for both protons and electrons. Solar proton fluences are treated statistically, using historical data to provide the probability of particle fluxes as a function of energy and mission duration [33].

The models can also be used to predict the long-term dose for spacecraft orbits where few measurements have been made. Typically, the trapped, radiation-belt models are used to generate the average electron and proton spectra for a one-year exposure. This is then multiplied by the number of years planned for the mission to give the expected radiation-belt contribution to the total radiation dose. The solar proton dose is calculated separately, and added to the radiation-belt contribution to give the total radiation dose. Particle-transport codes are used to propagate the particles through the spacecraft's shielding. They also keep track of the X-rays and gamma rays (bremsstrahlung) produced by the particles as they pass through material. The codes then add up the energy that is transmitted through the shielding into the underlying materials or devices. This energy is usually expressed as the absorbed dose for silicon (the most common material in microcircuits). The result provides an estimate of the shielding provided by a design for protecting electronics and other items (solar arrays, optics, humans, etc.) from the radiation that will be accumulated in that orbit during a mission.

The satellite designer will normally select parts that have been tested for total radiation dose and for single-event effects. He or she will know the intrinsic hardness of the parts in kilorads. He or she will then use curves, such as those shown in Figure 12, to select the additional shielding required for the orbit and the planned duration of the mission. Figure 12 shows the results of a total radiation dose calculation for satellites in geosynchronous, Molniya, and GPS orbits. The values are given in rads/year, and are assumed to be about the same at any time during a solar cycle. Missions are presently being planned to survive for 15 or more years.

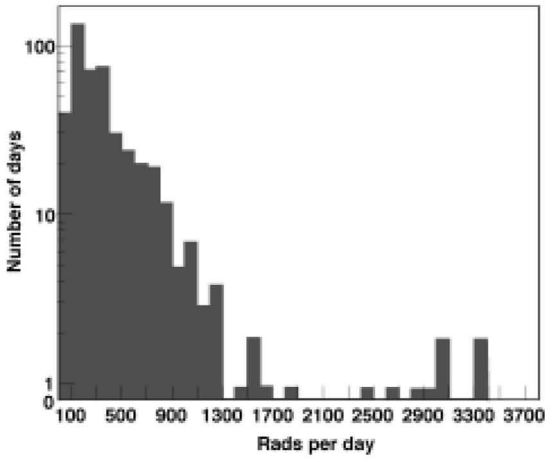

Figure 13. A histogram of the daily electron dose rate experienced in a GPS orbit over a 13-month period.

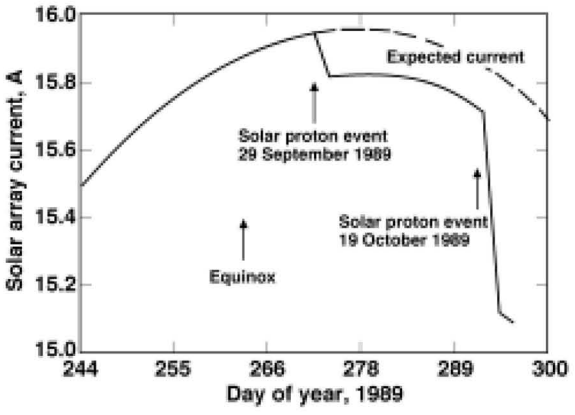

Figure 14. The solar-array current observed on GOES-7 during the fall of 1989 (after [35], reprinted with permission of the American Institute of Aeronautics and Astronautics, Inc.).

3.4.3 Electron Radiation Dosage in GPS Orbit

Some GPS satellites have carried dosimetry to verify the model predictions for total radiation dose for the GPS orbit. Figure 13 shows the dose in rads/day behind a 75-mil aluminum shield during about a thirteen-month period While the long-term average dose was close to the expected value, the day-to-day and week-to-week variations were large. Sometimes, the peaks and valleys in the dose rate were more than an order of magnitude greater or less than the average. Most of the dose-rate variations experienced by this GPS satellite were caused by variations in the trapped energetic electron fluxes. The high values of the dose rate dominated the long-term average. That is, the majority of total dose could be accumulated in a relatively short time, especially if a succession of storms occurred. The peak dose rates might also be hazardous for devices with marginal radiation or dose-rate tolerance.

3.5 Solar-Cell Degradation

Energetic protons from solar particle events damage solar arrays and reduce their ability to generate current [34]. This can significantly reduce the lifetime of a communications satellite. Solar arrays are covered with thin glass covers to shield the solar cells from all protons with energies < 10 MeV, because at geosynchronous orbit there are very few trapped protons with energies > 10 MeV. However, solar proton events can generate high fluences of > 10 MeV protons in a few days. The fluence of > 50 MeV protons can be substantial. As an example, the GOES 7 solar array current was reduced by nearly 10% as a result of two large solar proton events in 1989, as shown in Figure 14 [35].

3.6 Atmospheric Effects

During storms, the upper atmosphere heats and expands in response to increases in auroral currents, solar X-rays, solar ultraviolet radiation, and the precipitation of radiation-belt and plasma-sheet particles into the atmosphere. During a large storm, the density of the neutral atmosphere at Shuttle and space-station altitudes may reach 100 times its quiet-time value. These episodic increases in the atmospheric density are superimposed upon longer-term trends in the overall heating and expansion of the atmosphere in response to the 11-year solar cycle.

Low-altitude satellite orbits are always decaying, due to atmospheric drag. The increased atmospheric densities from the increase of the solar ultraviolet emissions during the peaks of the solar cycle and during large geomagnetic disturbances can cause significant ephemeris errors, and can hasten the decay of satellites. Figure 15 shows the satellite-tracking problems caused by such ephemeris errors due to increased drag during the large magnetic storm of March, 1989 [36]. The temporal profile of the storm is given by the Daily Magnetic Index, Ap. This showed a peak in magnetic activity on March 13. The histogram showed that the tracking problems began as the storm was subsiding, and lasted for about a week before all of the spacecraft (including large debris) was located and identified. Although this does not affect geosynchronous spacecraft, it does cause tracking errors that can lead to failures to acquire telemetry or transponder signals for low-altitude spacecraft, such as those used by radio amateurs.

4. Solar-Cycle Effects

Sunspots have been monitored for over 250 years. The official international Sunspot Number is issued by the Solar Index Data Center [37]. The times of the solar

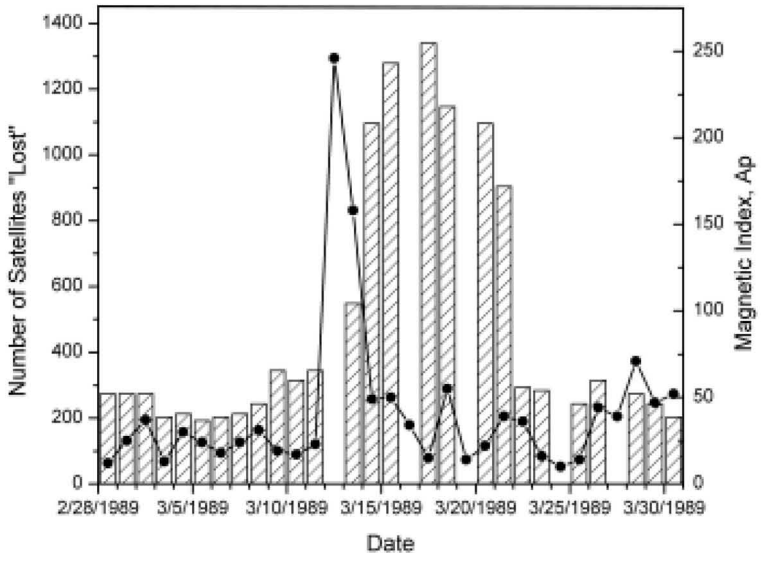

Figure 15. Satellite tracking problems after the March 13-14, 1989 magnetic storm. The histogram shows the number of satellites the tracks of which were lost as a result of the atmospheric disturbances caused by this severe storm [36]. The storm intensity was measured by the daily magnetic index, Ap.

maximum and solar minimum are based on the thirteen-month, running, smoothed, sunspot numbers. The number of sunspots varies with a cycle that has a period of about eleven years. This is known as the solar cycle. The current cycle is Solar Cycle 23. It began at solar minimum in 1996 and peaked in April of 2000. The next minimum is currently predicted to occur in December 2006. The maximum, smoothed, sunspot number varies by a factor of about five from the lowest to the highest, for the 23 cycles to date.

A number of solar and geomagnetic activity parameters are shown in Figure 16. The upper-left panel shows that the number of optical solar flares correlates closely with the sunspot number. But the hazards do not correlate so well with the sunspot number. For example, moderate to severe geomagnetic storms, shown in the lower-left panel, show only a weak relationship to the solar cycle. Nymmik [38] has shown that the number of solar particle events per year is very nearly a linear function of the average sunspot number. However, the distribution for the number of events per year as a function of the > 30 MeV proton fluence is independent of the sunspot number. Thus, the number of events maximizes at solar maximum, but a severe event can occur at any time during the solar cycle. Wren et al. [5, 39] have shown that the number of anomalies attributed to internal charging on a geosynchronous communications satellite is at a minimum during solar maximum, and maximizes during the declining phase of the solar cycle. They showed that this generally agrees with the variation in the two-day fluence of > 2 MeV electrons, as measured by the GOES spacecraft in geosynchronous orbit.

Spacecraft design must be based on worst-case estimates for each of the hazards, since each can have extreme levels at any time during a solar cycle. For high reliability, a short spacecraft mission around solar minimum must have the same protection as a long mission spanning more than one solar cycle, for all hazards except total radiation dose. Even for that, it must be protected against a major solar proton event.

5. Extreme Events and Anomalies

Examination of more than a solar cycle of the GOES daily-average electron flux data indicates that the extended period of energetic-electron flux enhancements in early 1994 was exceptional during solar cycle 22. However, the 1994 fluxes were not the highest. The highest daily-average electron fluxes observed by GOES occurred in response to a large solar event and magnetic storm that happened in late March, 1991. The distribution of daily average flux levels showed that they exceeded 10^4 electrons/(cm^2-s) about 6% of the time.

The statistics of extreme values can be used to study the extreme values that can be expected for the integral flux of energetic electrons in geosynchronous orbit. Using a data set that extended from January 1, 1986, through August 31, 1999, Koons [40] used extreme-value analysis to show that the extreme values fitted a generalized Pareto distribution [41], with an upper end point at an average daily flux of 2.34×10^5 electrons/(cm^2-s). The largest sample in the 13.67-year data set was 7.94×10^4 electrons/(cm^2-s) on March 28, 1991. A large storm in July, 2004, produced a higher daily-average flux of 9.63×10^4 electrons/(cm^2-s) on July 29. The analysis by Koons gave an expected value of 9.57×10^4 electrons/(cm^2-s) for a 50-year storm and 1.08×10^5 electrons/(cm^2-s) for a 100-year storm. Because the electron data were taken by sensors on different spacecraft in 1991 and 2004, caution must be exercised in comparing the data.

Severe space-weather events are expected to cause an increase in anomalies on spacecraft in most orbits. Information from NASA Earth and space-science missions from the severe storm period from October 19 to November 4, 2003, indicated that 59% of the spacecraft and about 18% of the instrument groups experienced some effect from the solar activity. Spacecraft-by-spacecraft details were given in [42].

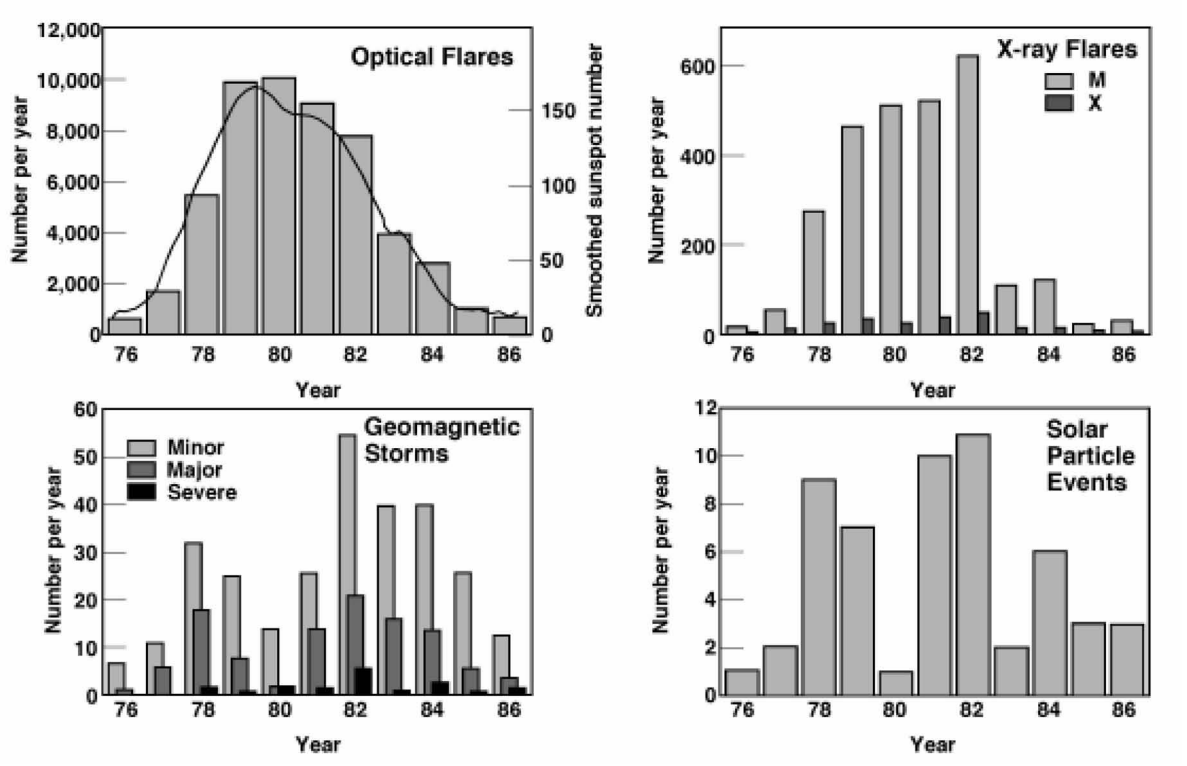

Figure 16. The solar and geomagnetic activity parameters for Solar Cycle 21. The solar cycle is shown by the curve for the smoothed sunspot number in the upper-left panel (courtesy of NOAA).

6. Conclusions

Space weather continues to be a serious hazard to modern communications spacecraft. The most serious effect is loss of mission. However, millions of dollars are spent addressing the design problems associated with the interaction of the space environment with spacecraft. Specification models are available for most of the phenomena. However, only about 40 years of data have been collected – none continuously. What has been collected and is available is insufficient to accurately specify, even in a statistical sense, the environment to be expected during a specific mission. We frankly don't know the size of the worst environment that the sun can throw at us. It is essential that high-quality data be continuously collected on each of the phenomena, and that we continue to make the effort to better understand the interaction of each with spacecraft materials and components, if we wish to design spacecraft that are safe from the environment.

7. Acknowledgements

The authors wish to thank James L. Roeder and Paul O'Brien for helpful discussions. This work was supported in part by The Aerospace Corporation IR&D Program, and in part by NASA Grant NAG5-10938.

8. References

1. A. C. Clarke, "Extra-Terrestrial Relays," *Wireless World,* October 1945, pp. 305-308.
2. B. F. James, O. W. Norton, and M. B. Alexander, "The Natural Space Environment: Effects on Spacecraft," *NASA Reference Publication 1350,* November 1994 (available from National Aeronautics and Space Administration, Marshall Space Flight Center, MSFC, Alabama 35812 USA).
3. R. D. Leach and M. B. Alexander, "Failures and Anomalies Attributed to Spacecraft Charging," *NASA Reference Publication 1375,* August 1995 (available from National Aeronautics and Space Administration, Marshall Space Flight Center, MSFC, Alabama 35812 USA).
4. K. L. Bedingfield, R. D. Leach, and M. B. Alexander, "Spacecraft System Failures and Anomalies Attributed to the Natural Space Environment," *NASA Reference Publication 1390*, August 1996 (available from National Aeronautics and Space Administration, Marshall Space Flight Center, MSFC, Alabama 35812 USA).
5. G. L. Wrenn, "Conclusive Evidence for Internal Dielectric Charging Anomalies on Geosynchronous Communications Spacecraft," *Journal of Spacecraft and Rockets,* **32,** 3, 1995, pp. 514-520.
6. J. H. Allen and D. C. Wilkinson, "Solar-Terrestrial Activity Affecting Systems in Space and on Earth," in J. Hruska, M. A. Shea, D. F. Smart, and G. Heckman (eds.), *Solar-Terrestrial Predictions – IV, Proceedings of a Workshop at Ottawa, Canada, May 18-22, 1992*, Vol. 1, September 1993, pp. 75-107 (available from National Oceanic and Atmospheric Administration, Environmental Research Laboratories, Boulder, CO, USA).
7. H. C. Koons, J. E. Mazur, R. S. Selesnick, J. B. Blake, J. F. Fennell, J. L. Roeder, and P. C. Anderson, "The Impact of the

Space Environment on Space System," *Aerospace Report No. TR-99(1670)-1*, The Aerospace Corporation, El Segundo, CA, 1999.
8. H. C. Koons, J. E. Mazur, R. S. Selesnick, J. B. Blake, J. F. Fennell, J. L. Roeder, and P. C. Anderson, "The Impact of the Space Environment on Space System," in Proceedings of the 6th Spacecraft Charging Technology Conference, November 2-6, 1998, *AFRL-VS-TR-20001578*, Air Force Research Laboratory, Hanscom, MA, September 2000, pp. 55-59, pp. 7-11.
9. J. F. Fennell, J. L. Roeder, and H. C. Koons, "Substorms and Magnetic Storms from the Satellite Charging Perspective," in Ling-Hsiao Lyu (ed.), *Space Weather Study Using Multipoint Techniques, Proceedings of the COSPAR Colloquium*, Taipei, Taiwan, September 27-29, 2000, Amsterdam, Pergamon, 2002, pp. 163-173.
10. J. H. Adams, Jr., R. Silberberg, and C. H. Tsao, "Cosmic Ray Effects on Microelectronics," *IEEE Transactions on Nuclear Science*, **NS-29**, 1, 1982, 169-172.
11. E. Normand, "Single-Event Effects in Avionics," *IEEE Transactions on Nuclear Science*, **43**, 2, 1996, pp. 461-474.
12. C. Barillot and P. Calvel, "Review of Commercial Spacecraft Anomalies and Single-Event-Effect Occurrences," *IEEE Transactions on Nuclear Science*, **43**, 2, 1996, pp. 453-460.
13. D. F. Smart and M. A. Shea, "Chapter 6: Galactic Cosmic Radiation and Solar Energetic Particles," in A. S. Jursa (ed.), *Handbook of Geophysics and the Space Environment*, pp. 6-1-6-29, Air Force Geophysics Laboratory, Air Force Systems Command, United States Air Force, 1985, (available from the National Technical Information Service, Springfield, VA 22161 USA).
14. J. H. Adams, Jr., R. Silberberg, and C. H. Tsao, "Cosmic Ray Effects on Microelectronics, Part I: The Near-Earth Particle Environment," *NRL Memorandum Rpt. 4506*, August 1981.
15. H. C. Koons and M. W. Chen, "An Update on the Statistical Analysis of MILSTAR Processor Upsets," in *1999 Government Microcircuit Applications Conf., Digest of Papers*, **24**, March 1999, pp. 816-819.
16. *S. E. C. User Notes*, Issue 28, NOAA, Space Environment Center, Boulder, CO, January 2000.
17. W. N. Spjeldvik and P. L. Rothwell, "Chapter 5: The Radiation Belts," in A. S. Jursa (ed.), *Handbook of Geophysics and the Space Environment*, p. 5-28, Air Force Geophysics Laboratory, Air Force Systems Command, United States Air Force, 1985, (available from the National Technical Information Service, Springfield, VA 22161 USA).
18. J. H. Allen, "Satellite Anomalies, Recent Events, and Possible Causes," *Space Weather Study Using Multipoint Techniques, Proceedings of the COSPAR Colloquium*, Taipei, Taiwan, September 27-29, 2000, (available from the SCOSTEP website homepage at http://www.ngdc.noaa.gov/stp/SCOSTEP/scostep.html), slide 50.
19. I. Katz, M. Mandell, G. Jongeward, and M. S. Gussenhoven, "The Importance of Accurate Secondary Electron Yields in Modeling Spacecraft Charging," *Journal of Geophysical Research*, **91**, 12, 1986, pp. 13739-13744.
20. R. D. Leach and M. B. Alexander, "Failures and Anomalies Attributed to Spacecraft Charging," *NASA Reference Publication 1375*, August 1995, p. 16, (available from National Aeronautics and Space Administration, Marshall Space Flight Center, MSFC, Alabama 35812 USA).
21. H. C. Koons and D. J. Gorney, "The Relationship Between Electrostatic Discharges on Spacecraft P78-2 and the Electron Environment," *Journal of Spacecraft and Rockets*, **28**, 6, 1991, pp. 683-688.
22. P. C. Anderson, "Surface Charging in the Auroral Zone on the DMSP Spacecraft in LEO," in Proceedings of the 6th Spacecraft Charging Technology Conference, November 2-6, 1998, *AFRL-VS-TR-20001578*, Air Force Research Laboratory, Hanscom, Mass., September 2000, pp. 55-59.
23. P. C. Anderson and H. C. Koons, "Spacecraft Charging Anomaly on a Low-Altitude Satellite in an Aurora," *Journal of Spacecraft and Rockets*, **33**, 5, 1996, pp. 734-738.
24. M. S. Gussenhoven, D. A. Hardy, F. rich, W. J. Burke, and H. -C. Yeh, "High Level Charging in the Low-Altitude Polar Auroral Environment," *Journal of Geophysical Research*, **90**, A11, 1985, pp. 11000-11023.
25. H. E. Spence, J. B. Blake, and J. F. Fennell, "Surface Charging Analysis of High-Inclination, High-Altitude Spacecraft: Identification and Physics of the Plasma Source Region," *IEEE Transactions on Nuclear Science*, **40**, 6, 1993, pp. 1521-1524.
26. J. J. Capart and J. J. Dumesnil, "The Electrostatic-Discharge Phenomena on Marecs-A," *ESA Bulletin*, No. 34, May 1983, pp. 22-27.
27. M. Frezet, E. J. Daly, J. P. Granger, and J. Hamelin, "Assessment of Electrostatic Charging of Satellites in Geostationary Environment," *ESA Journal*, **13**, 2, 1989, pp. 89-116.
28. J. I. Vette, "*The AE-8 Trapped Electron Model Environment*," NSSDC/WDC-A-R&S 91-24, Goddard Space Flight Center, MD, 1991.
29. A. L. Vampola, "Thick Dielectric Charging on High-Altitude Spacecraft," *Journal of Electrostatics*, **20**, 1987, pp. 21-30.
30. H. C. Koons, J. E. Mazur, R. S. Selesnick, J. B. Blake, J. F. Fennell, J. L. Roeder, and P. C. Anderson, "The Impact of the Space Environment on Space System," *Aerospace Report No. TR-99(1670)-1, Appendix A*, The Aerospace Corporation, El Segundo, CA, 1999, pp. 7-9.
31. D. C. Mayer and R. C. Lacoe, "Designing Integrated Circuits to Withstand Space Radiation," *Crosslink*, The Aerospace Corporation, **4**, 2, 2003, pp. 30-35.
32. D. M. Sawyer and J. I. Vette, "AP-8 Trapped Proton Environment," *NSSDC/WDC-A-R&S 76-06*, Goddard Space Flight Center, MD, 1976.
33. J. Feynman, G. Spitale, J. Wang, and S. Gabriel, "Interplanetary Proton Fluence Model: JPL 1991," *Journal of Geophysical Research*, **98**, 8, 1993, pp. 13281-13294.
34. L. J. Lanzerotti, D. W. Mauer, H. H. Sauer, and R. D. Zwickl, "Large Solar Proton Events and Geosynchronous Communication Spacecraft Solar Arrays," *Journal of Spacecraft and Rockets*, **28**, 5, 1991, pp. 614-616.
35. D. C. Marvin and D. J. Gorney, "Solar Proton Events of 1989: Effects on Spacecraft Solar Arrays," *Journal of Spacecraft and Rockets*, **28**, 6, 1991, pp. 713-719.
36. D. J. Gorney, H. C. Koons, and R. L. Walterscheid, "Some Prospects for Artificial Intelligence Techniques in Solar-Terrestrial Prediction," *Solar-Terrestrial Predictions – IV, Proceedings of a Workshop at Ottawa, Canada, May 18-22, 1992*, Vol. 2, September 1993, pp. 550-564 (available from National Oceanic and Atmospheric Administration, Environmental Research Laboratories, Boulder, CO, U.S.A.).
37. Solar Index Data Center, Royal Observatory of Belgium, Av. *Circulaire*, **3**, B-1180 Brussels, Belgium.
38. R. A. Nymmik, "Relationships among Solar Activity, SEP Occurrence Frequency, and Solar Energetic Particle Event Distribution Functions," *Proc. 26th International Cosmic Ray Conference*, **6**, 1999, pp. 280-283.
39. G. L. Wrenn, D. J. Rodgers, and K. A. Ryden, "A Solar Cycle of Spacecraft Anomalies Due to Internal Charging," *Annales Geophysicae*, **20**, 2002, pp. 953-956.
40. H. C. Koons, "Statistical Analysis of Extreme Values in Space Science," *Journal of Geophysical Research*, **106**, A6, 2001, pp. 10915-10921.
41. R. -D. Reiss and M. Thomas, *Statistical Analysis of Extreme Values*, Boston, MA, Birkhäuser Verlag, 1997.
42. L. P. Barbieri and R. E. Mahmot, "October-November 2003's Space Weather and Operations Lessons Learned," *Space Weather*, **2**, 2004, pp. 15-29, doi:10.1029/2004SW000064.